



Efficient generation of broadband short-wave infrared vector beams with arbitrary polarization

Cite as: Appl. Phys. Lett. **114**, 021107 (2019); <https://doi.org/10.1063/1.5082809>

Submitted: 25 November 2018 . Accepted: 30 December 2018 . Published Online: 17 January 2019

Tong Li , Zhancheng Li, Shuqi Chen, Lyu Zhou, Nan Zhang, Xin Wei , Guofeng Song, Qiaoqiang Gan, and Yun Xu



View Online



Export Citation



CrossMark

ARTICLES YOU MAY BE INTERESTED IN

[Enhanced quantum dots spontaneous emission with metamaterial perfect absorbers](#)

Applied Physics Letters **114**, 021103 (2019); <https://doi.org/10.1063/1.5081688>

[Thermal bistability of magnon in yttrium iron garnet microspheres](#)

Applied Physics Letters **114**, 021101 (2019); <https://doi.org/10.1063/1.5075503>

[A simple approach to fiber-based tunable microcavity with high coupling efficiency](#)

Applied Physics Letters **114**, 021106 (2019); <https://doi.org/10.1063/1.5083011>



Measure Ready
M91 FastHall™ Controller

A revolutionary new instrument
for complete Hall analysis

 Lake Shore
CRYOTRONICS

Efficient generation of broadband short-wave infrared vector beams with arbitrary polarization

Cite as: Appl. Phys. Lett. **114**, 021107 (2019); doi: [10.1063/1.5082809](https://doi.org/10.1063/1.5082809)

Submitted: 25 November 2018 · Accepted: 30 December 2018 · Published Online: 17 January 2019





View Online



Export Citation



CrossMark

Tong Li,^{1,2,3}  Zhancheng Li,⁴ Shuqi Chen,^{4,5} Lyu Zhou,⁶ Nan Zhang,⁶ Xin Wei,^{1,2,3}  Guofeng Song,^{1,2,3} Qiaoqiang Gan,^{6,7} and Yun Xu^{1,2,3,a)}

AFFILIATIONS

¹ Institute of Semiconductors, Chinese Academy of Sciences, Beijing 100083, China

² College of Materials Science and Opto-Electronic Technology, University of Chinese Academy of Sciences, Beijing 100049, China

³ Beijing Key Laboratory of Inorganic Stretchable and Flexible Information Technology, Beijing 100083, China

⁴ The Key Laboratory of Weak Light Nonlinear Photonics, School of Physics and TEDA Institute of Applied Physics, Nankai University, Tianjin 300071, China

⁵ The collaborative Innovation Center of Extreme Optics, Shanxi University, Taiyuan, Shanxi 030006, China

⁶ Department of Electrical Engineering, The State University of New York at Buffalo, Buffalo, New York 14260, USA

⁷ School of Optical-Electrical and Computer Engineering, University of Shanghai for Science and Technology, Shanghai 200093, China

^{a)} Author to whom correspondence should be addressed: xuyun@semi.ac.cn.

ABSTRACT

Vector beams have shown great promise for applications ranging from near-field optics to nonlinear optics. Here, we experimentally demonstrate a highly efficient and broadband metasurface-based polarization converter that can realize linear polarization rotation with more than 0.9 conversion efficiency over a 1300 nm bandwidth in the short-wave infrared band. Building upon this broadband polarization converter, we design a meta-reflectarray that is capable of generating arbitrary vector beams with the efficiency of >0.8 from 1200 nm to 2500 nm and therefore enable a wide range of applications including optical imaging, optical communication, and data encryption.

Published under license by AIP Publishing. <https://doi.org/10.1063/1.5082809>

Vector beams (VBs) have gained more significant attention due to the inhomogeneous polarization distribution of the transverse plane. The applications of VBs have been reported in focus shaping,^{1–3} optical trapping,^{4–6} near-field optics,⁷ optical imaging,^{8,9} and nonlinear optics.^{10–12} Many approaches have been explored to generate VB, including birefringence in crystal and polymers,¹³ laser resonators,^{14,15} spatial light modulation,^{16,17} and the integration of optical elements into the output surface of semiconductor lasers.¹⁸ However, conventional optical components greatly suffered from narrow bandwidths and bulky footprints, imposing barriers for miniaturization and integration of optical systems. Furthermore, the severe energy loss of bulky optical components is still a defect in practical applications. Recently, metamaterials have attracted widespread research interest due to their unique ability to precisely manipulate electromagnetic waves. As a planar version of metamaterials with a

subwavelength thickness, metasurfaces are broadly used in light polarization applications. Many works have been made in generating the VB with various nanoparticle arrays.^{19–23} However, all of these suffer from a complex fabrication process and a relatively narrow bandwidth. Generating the VB in the broadband is an urgent issue.

In this work, we propose and experimentally demonstrate a high-efficiency and broadband, short-wave infrared (SWIR) polarization converter using compact reflective metasurfaces. The proposed metasurface consists of eight groups of rectangular nanoparticle arrays with different azimuth angles. By meticulously arranging the position of arrays on the metasurface, VB with arbitrary polarization distribution can be achieved with the reflection efficiency >0.8 over a broadband ranging from 1200 nm to 2500 nm; meanwhile, the polarization conversion efficiency >0.9 . The proposed method provides capabilities for

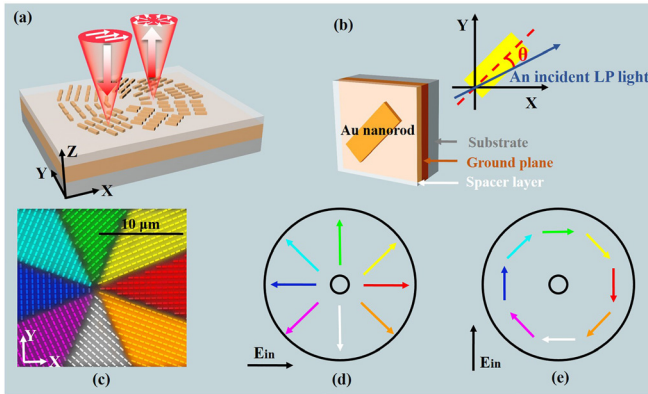


FIG. 1. (a) Schematic of generating VB through a metasurface. (b) The unit cell of the metasurface consists of three layers: the ground gold plane, the SiO₂ spacer layer, and the top layer of gold nanorods. The thickness of each layer is 150 nm, 200 nm, and 50 nm, respectively. Each pixel size is 650 nm by 650 nm. Each nanorod is 540 nm in length and 180 nm in width. The inset shows the optical axis azimuth θ of the nanorod. (c) SEM image of the metasurface for generating arbitrary VB. Local magnification is shown in the inset (scale bar: 10 μm). Schematic representation of the polarization distribution of the (d) radially polarized vector beam and (e) azimuthally polarized vector beam.

the development of compact devices, which may lead to advancement in a wide range of fields in optics and photonics.

Figure 1(a) shows the schematic of the VB generator: A linear polarized (LP) incident light can be converted to a VB reflected by the metal-insulator-metal (MIM) metasurface. As illustrated in Fig. 1(b), the MIM is composed of a gold (Au) ground plane, a silica spacer layer, and a layer of aligned gold rectangular antennas (the details of the fabrication process are given in Sec. 1 in the [supplementary material](#)). Here, we define θ to describe the angle between the long axis of the rectangular nanoparticle and the polarization direction of incident LP light. The VB metasurface is constructed by Au nanoparticle arrays with different θ values. Upon the illumination of an LP light, an arbitrary LP optical rotation can be realized using various Au nanoparticle arrays. Therefore, the reflected VB is a combination of multiple LP beams with different polarization distributions. The false colored scanning electron microscopy (SEM) image of the fabricated VB metasurface is shown in Fig. 1(c). By controlling and optimizing the geometric parameters of each section of this VB metasurface, arbitrary VB over a broadband in the SWIR regime can be obtained depending on the polarization direction of the incident LP beam. For instance, a standard radially polarized vector beam (or an azimuthally polarized vector beam) can be obtained under the illumination of an LP light with the

polarization along the x axis (or the y axis). The model of the polarization patterns is illustrated in Figs. 1(d) and 1(e), respectively. The colored arrows correspond to the polarization direction of reflected LP light generated by each Au array. Next, we will explain the design principle of this type of VB metasurface, starting from the thin-film half-wave plate metasurface.

The half-wave plate is one of the most fundamental components in polarization optics. The principle of generating VB is based on the optical rotation of a half-wave plate. Here, we demonstrate an efficient, broadband half-wave plate in the SWIR range using an ultrathin metasurface with its optical axis along the 45° axis, as shown in Fig. 2(a). The reflection spectra of the half-wave plate sample were experimentally characterized using a Fourier-transform IR spectrometer (VERTEX 70, Bruker Optics). The incident LP beam was normal to the sample surface with the polarization direction along the x axis. As a result, the incident LP light is converted into its cross-polarized light (R_{cross}) and co-polarized light (R_{co}). The reflectance for both polarizations is shown in Fig. 2(b). One can see that the cross-polarized reflection is about 0.8 from 1200 nm to 2500 nm. In contrast, the co-polarized reflection is mostly lower than 0.17. The corresponding polarization conversion rate (PCR), defined as $\text{PCR} = R_{\text{cross}} / (R_{\text{cross}} + R_{\text{co}})$, is also calculated as a function of wavelength, as shown in Fig. 2(c). The experimental results showed that the PCR remains above 0.9, nearly covering the entire SWIR band, which agrees well with the simulation result (see details of modeling in the [supplementary material](#), Sec. II). Therefore, our numerical simulations and optical characterization results show that the polarization conversion efficiency is over 0.9 with 0.8 reflectance across a 1300 nm bandwidth. The broadband operation results from the superposition of multiple resonance peaks (see the principle of high efficiency and broadband half-wave plate metasurface in the [supplementary material](#), Sec. III).

Strictly speaking, the arbitrary VB needs 0°–360° polarization direction distribution. It is worth noting that arbitrary LP distribution can be obtained by properly tuning the designed half-wave plate metasurface. Due to the anisotropic resonance of rectangular nanoparticles, the amplitude and phase of the orthogonal electric field components can be tuned easily by changing the azimuth angle θ of the nanoparticles. That is to say, a different reflected LP beam can be composed. To interpret the polarization conversion performance of the half-wave metasurface, we calculate the optical rotation angle Ψ , the degree of linear polarization (DOLP), and the reflectivity of the reflected light as a function of θ in a wavelength range from 1200 nm to 2500 nm. Here, we maintain the polarization direction of the incident LP light along the x -axis and control the azimuth angles

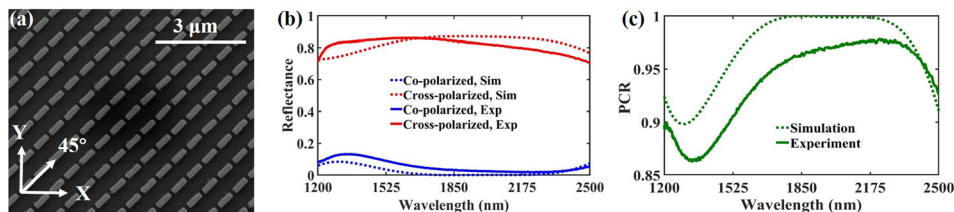


FIG. 2. (a) The SEM image of the half-wave plate metasurface. (b) Simulated and experimental reflectance spectra of co-polarized and cross-polarized light at normal incidence. (c) Simulated and experimental polarization conversion efficiency at normal incidence.

θ by rotating the long axis of the Au nanoparticles. Ψ is defined as the angle difference between the polarization direction of the reflected light and the x-axis

$$\tan 2\Psi = \frac{2E_x E_y \cos(\Delta\varphi)}{E_x^2 - E_y^2}, \quad (1)$$

where E_x and E_y represent the amplitude of the co-polarized and cross-polarized components, respectively. $\Delta\varphi = \varphi_x - \varphi_y$ is the phase difference between co-polarized and cross-polarized components. As illustrated in Fig. 3(a), it is obvious that the value of Ψ can be tuned from 90° to -90° by adjusting θ . As shown by the white dotted line at a wavelength of 1550 nm, the value of Ψ as a function of azimuth angle θ is extracted and plotted in Fig. 3(b), and the optical rotation angle Ψ can be tuned in the range of -90° to 90° . It is worth noting that the azimuth angle θ and the azimuth angle $\theta + 90^\circ$ correspond to the same Ψ , but the phase information of Ψ is different. Figure 3(c) shows the calculated phase values of Ψ as a function of θ at a wavelength of 1550 nm. For simplicity, we use A, B, C, and D to represent different ranges of θ . It can be clearly seen that the reflected waves have the same phase when θ located in region B and region C (region A and region D). However, the phase in region A and region D has a π phase delay relative to region B and region C. Therefore, the azimuth angle difference of 90° will result in a π phase difference of Ψ . By introducing a π phase delay in the reflected wave, the coverage of the optical rotation angle Ψ will be extended from -180° to 180° , that is, from 0° to 360° .

Furthermore, we also calculated the value of DOLP, which can be expressed as

$$\text{DOLP} = \frac{\sqrt{(E_x^2 - E_y^2)^2 + (2E_x E_y \cos(\Delta\varphi))^2}}{E_x^2 + E_y^2}. \quad (2)$$

The DOLP is often used to evaluate the quality of linear polarization. In Fig. 3(d), the DOLP values of reflected waves are larger than 0.9 from 1420 nm to 2500 nm, which can be considered as perfect LP light.²⁴ Because the co-polarized component is not completely converted to the cross-polarized component in a wavelength range from 1200 nm to 1420 nm, the DOLP values

are less than 0.9 but greater than 0.8, which can still be treated as LP light. Therefore, the obtained reflected light exhibits a great linear polarization state. Finally, we calculate the reflectivity of the reflected beams, as shown in Fig. 3(e). The maximum reflectivity of the designed metasurface can reach up to 0.9, while the minimum reflectivity is still above 0.7. The reflectivity is mainly restricted by ohmic loss in metallic antennas, and the antenna's LSPR in the x-direction changes with the rotation of Au nanorods. Ohmic loss decreases as the value of θ tunes from 0° to 90° (from 0° to -90°), i.e., reflectivity increases. Hence, an efficient and broadband arbitrary optical rotation with high DOLP can be realized by rotating the half-wave plate metasurface systems. Here, we listed eight units, for units 1–8, given θ of 0° , 22.5° , 45° , 67.5° , 90° , -67.5° , -45° , and -22.5° , the Ψ of 0° , 45° , 90° , 135° , 180° , 225° , 270° , and 315° can be obtained, respectively. Therefore, the VB with a variety of polarization distributions can be realized with a flexible combination of these discrete units. Additionally, the ultra-wide band of the 0° to 360° polarization rotation indicates that VB can also be realized in a broad wavelength range.

To demonstrate the ability of the designed metasurface to convert an LP beam to an arbitrary VB over a broad bandwidth, the reflected VB light under the vertical incident LP waves was characterized using an optical system as shown in Fig. 4(a). The light source was a supercontinuum laser (NKT SuperK EXR-20). Its beam collimated by a fiber collimator then passed through an infrared polarizer (P_1) and a beam splitter. Afterwards, the beam was focused on metasurfaces by a long-working-distance objective (Sigma NIR plan apo 10x, NA = 0.3). We inserted an additional infrared polarizer (P_2) to analyze the polarized state of the reflective wave. The VB pattern was obtained with an InGaAs camera (HAMAMATSU InGaAs C10633). The intensity profiles of VB were measured at the wavelength of 1550 nm, as displayed in Fig. 4(b). By changing the polarization direction of the incident LP beam, different VBs could be obtained. The polarization direction of the incident light was indicated by P_1 (brown double-head arrows). The images of the reflected light show various patterns for different directions of P_2 (blue double-head arrows). Specifically, when the polarization direction of P_1 is parallel to the x axis, it is obvious that a two-fan pattern is arranged

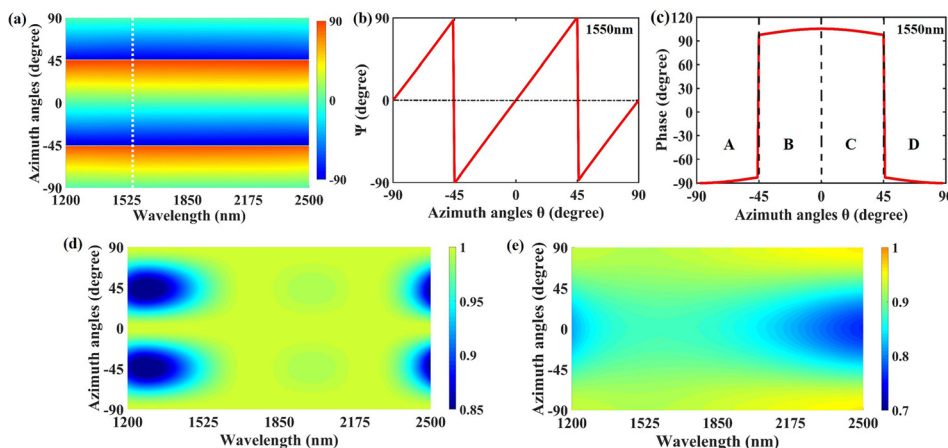


FIG. 3. Illustration of the polarization conversion of the emerging light. The incident light is x-polarized. (a) Rotation angles. (b) Rotation angles as a function of θ at a wavelength of 1550 nm. (c) The phase of rotation angles. The variation range of θ is divided into four regions: A (-90° to -45°), B (-45° to 0°), C (0° to 45°), and D (45° to 90°). The DOLP and reflectivity of rotation angles are shown in (d) and (e), respectively.

in the horizontal direction, which is parallel to the blue arrow when the polarization angles of P_2 equal 0° . When P_2 was rotated by 45° , 90° , and 135° , respectively, the two-fan pattern was also rotated in the same manner. That is, the direction of the reflected two-fan pattern is always parallel to the polarization direction of P_2 . The complete model of polarization distribution that resulted from the observation is depicted in Fig. 1(d). This result proves that the proposed metasurface really converts an LP beam into the radially polarized vector beam. For the same reason, when the polarization direction of P_1 is parallel to the y axis, the reflected two-fan pattern is always perpendicular to the polarization direction of P_2 . Therefore, the polarization state of patterns is always perpendicular to the radius, which indicated that the reflected light is the azimuthally polarized vector beam. In the case when the polarization direction of P_1 is at an angle of 45° to the x -axis, the azimuth angles θ for units 1–8 became -45° , -22.5° , 0° , 22.5° , 45° , 67.5° , 90° , and -67.5° , corresponding to the Ψ values of 315° , 0° , 45° , 90° , 135° , 180° , 225° , and 270° , respectively. The two-fan patterns are no longer parallel or perpendicular to the polarization direction of P_2 , creating an atypical vector beam. The VB patterns were also measured at different wavelengths of 1200 nm, 1310 nm, and 1650 nm (see Fig. S3 in the supplementary material). These results are the same as those in Fig. 4(b). They all prove that the designed metasurface can generate arbitrary VB over a broadband from 1200 nm to 1700 nm (i.e., the spectral limit of our optical system). From the numerical simulation results of optical rotation and the trend of experimental results, we can expect that our proposed metasurface has the ability to convert an LP beam into VB in the wavelength range from 1700 nm to 2500 nm.

It is important to mention that the VB can be considered as a construction of various LP lights. We can also realize arbitrary VB by changing the polarization direction of the incident LP light. Additionally, due to the flexibility of the unit cell, we can also rebuild VB metasurfaces to realize VB with more complex spatial polarization distribution, such as double mode,²³ triple mode, and arbitrary multifold mode VB.

In conclusion, we experimentally demonstrated an approach to generate arbitrary VB using a single ultrathin metasurface. This

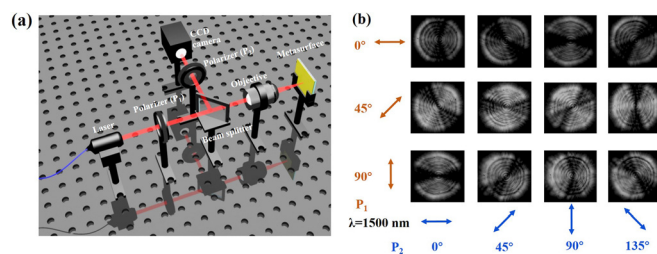


FIG. 4. Experimental VB measurement at a wavelength of 1550 nm. (a) Experimental setup for the reflection measurement. (b) The experimentally recorded intensity profile of the VB was measured as a function of different incident LP beams (brown double-headed arrow), with the analyzer P_2 aligned with the expected polarization direction (blue double-headed arrow). The measurements were performed under normal incidence. It is worth noting that the test pattern is mirror symmetrical with the actual pattern under the influence of the optical components in the measure system. Here, we show the actual patterns.

method is based on the coupling effect of the LP beam-dependent phase and polarization. The polarization states are manipulated by a single metasurface which consists of nanorods with spatially varying orientations. The reflectivity of our metasurface is more than 0.8 over a broadband ranging from 1200 nm to 2500 nm. Specifically, the polarization conversion efficiency is more than 0.9 over the most of band. Our work solves several major issues typically associated with VB generation, such as low conversion efficiency, narrow bandwidth, bulky size, and complicated experimental setup. The high reflectivity, polarization conversion efficiency, and tunable SWIR broadband make our metasurface promising for environmental remote sensing and military sensing. The proposed method provides capabilities for the development of compact devices, which may lead to advancement in a wide range of fields in optics and photonics.

See [supplementary material](#) for the manufacture process of the metasurface, simulation method, and principle of high efficiency and broadband half-wave plate metasurfaces and supplementary figures for measured VB patterns.

This work was supported by the National Basic Research Program of China (973 Program) (Nos. 2015CB351902 and 2015CB932402); Key Research Program of Frontier Sciences, the Chinese Academy of Sciences, Grant No. QYZDY-SSWJSC004; National Key R&D Program of China (Nos. 2016YFB0402400 and 2016YFB0400601); National Nature Science Foundation of China (No. U143231); and Beijing Science and Technology Projects (No. Z151100001615042). L. Zhou and Q. Gan acknowledge the funding support from the National Science Foundation of the U.S. (Grant Nos. CMMI1562057 and IIP-1718177).

REFERENCES

- ¹S. Zhou, S. Wang, J. Chen, G. Rui, and Q. Zhan, *Photonics Res.* **4**, B35 (2016).
- ²F. Kenny, D. Lara, O. G. Rodriguez-Herrera, and C. Dainty, *Opt. Express* **20**, 14015 (2012).
- ³J. Chen, J. Ng, Z. F. Lin, and C. T. Chan, *Nat. Photonics* **5**, 531 (2011).
- ⁴M. I. Marques, *Opt. Lett.* **39**, 5122 (2014).
- ⁵Y. Kozawa and S. Sato, *Opt. Express* **18**, 10828 (2010).
- ⁶G. H. Rui and Q. W. Zhan, *Nanophotonics* **3**, 351 (2014).
- ⁷A. Ciattoni, B. Crosignani, P. Di Porto, and A. Yariv, *Phys. Rev. Lett.* **94**, 073902 (2005).
- ⁸L. Novotny, M. R. Beversluis, K. S. Youngworth, and T. G. Brown, *Phys. Rev. Lett.* **86**, 5251 (2001).
- ⁹X. P. Li, T. H. Lan, C. H. Tien, and M. Gu, *Nat. Commun.* **3**, 998 (2012).
- ¹⁰A. Bouhelier, M. Beversluis, A. Hartschuh, and L. Novotny, *Phys. Rev. Lett.* **90**, 013903 (2003).
- ¹¹G. Rui, W. Chen, Y. Lu, P. Wang, H. Ming, and Q. Zhan, *J. Opt.* **12**, 035004 (2010).
- ¹²G. Bautista, J. Makitalo, Y. Chen, V. Dhaka, M. Grasso, L. Karvonen, H. Jiang, M. J. Huttunen, T. Huhtio, H. Lipsanen, and M. Kauranen, *Nano Lett.* **15**, 1564 (2015).
- ¹³F. Cardano, E. Karimi, S. Slussarenko, L. Marrucci, C. de Lisio, and E. Santamato, *Appl. Opt.* **51**, C1 (2012).
- ¹⁴Y. Kozawa and S. Sato, *Opt. Lett.* **30**, 3063 (2005).
- ¹⁵J. L. Li, K. Ueda, M. Musha, A. Shirakawa, and Z. M. Zhang, *Opt. Lett.* **32**, 1360 (2007).
- ¹⁶D. Xu, B. Gu, G. Rui, Q. Zhan, and Y. Cui, *Opt. Express* **24**, 4177 (2016).

- ¹⁷S. Liu, S. Qi, Y. Zhang, P. Li, D. Wu, L. Han, and J. Zhao, *Photonics Res.* **6**, 228 (2018).
- ¹⁸R. Chen, J. Wang, X. Zhang, A. Wang, H. Ming, F. Li, D. Chung, and Q. Zhan, *Opt. Lett.* **43**, 755 (2018).
- ¹⁹Q. Guo, C. Schlickriede, D. Wang, H. Liu, Y. Xiang, T. Zentgraf, and S. Zhang, *Opt. Express* **25**, 14300 (2017).
- ²⁰S. Kruk, B. Hopkins, I. I. Kravchenko, A. Miroshnichenko, D. N. Neshev, and Y. S. Kivshar, *APL Photonics* **1**, 030801 (2016).
- ²¹Y. Yang, W. Wang, P. Moitra, I. I. Kravchenko, D. P. Briggs, and J. Valentine, *Nano Lett.* **14**, 1394 (2014).
- ²²J. Li, S. Chen, H. Yang, J. Li, P. Yu, H. Cheng, C. Gu, H.-T. Chen, and J. Tian, *Adv. Funct. Mater.* **25**, 704 (2015).
- ²³P. Yu, S. Chen, J. Li, H. Cheng, Z. Li, W. Liu, B. Xie, Z. Liu, and J. Tian, *Opt. Lett.* **40**, 3229 (2015).
- ²⁴P. Yu, J. X. Li, C. C. Tang, H. Cheng, Z. C. Liu, Z. C. Li, Z. Liu, C. Z. Gu, J. J. Li, S. Q. Chen, and J. G. Tian, *Light: Sci. Appl.* **5**, e16096 (2016).